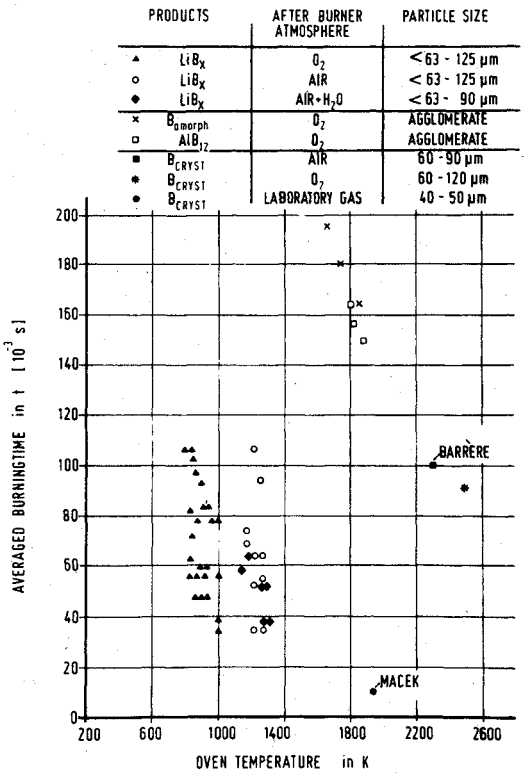

Fig. 5 The burning time of particles as a function of the oven temperature.

lithium could also be observed in the later phase of the particle burning-time. Thus a steady consumption of both the lithium and boron can be assumed for the main combustion. The findings of the spectral analysis were supported by the chemical analysis of the condensate from the quartz wall. Close to the exit of the oven, mainly lithium was identified. Further downstream in the combustion both lithium and boron could be detected.

The ignition delay time was plotted in Fig. 4. It varied from 30 msec Fig. 4 to 80 msec depending on the best conditions. The averaged burning time increased with increasing particle diameter. A comparison with the findings of other authors for pure boron was made in Fig. 5. The heat of combustion was measured in a calorimetric bomb to be 52.46 KJ/g.

Discussion

The ignition temperature of boron could be lowered from 2500 K to 800 K by using a $LiB_{2,5}$ compound. This ignition temperature was slightly increased by using air or humid air (90% moisture) instead of pure oxygen. The difficulties encountered for a complete combustion can best be discussed by using Table 1. The boiling temperature of the metal boron (3950 K) is much higher than that of the oxide B_2O_3 (2520 K) forming a dense layer above the melting point at 723 K. Therefore, a fast oxidation can only take place if the shielding oxide layer has been destroyed. The combined use of boron and lithium resulted in a very low ignition temperature (about 900°C in air) and complete combustion. The reaction mechanism was interpreted by the start-up phase of a lithium flame heating up the particle to the onset of the boron reaction. A closed oxide layer could not form as the lithium continued to vaporize or as lithiumborate was formed. All photographs showed a smooth combustion around the particles and no spinning traces as in the case of aluminum. These findings of good ignition and combustion properties together with a high heat of combustion justify further investigations of the B/Li compound as a prominent candidate for use within air-augmented propulsion systems.

References

[1] Schadow, K., "Study of Gaseous Nonequilibrium Effects in Particle-Laden, Ducted Flows for Improvement of the Combustion Efficiency," AIAA Paper 72-36 San Diego, Calif., 1972.

[2] Schadow, K., "The Influence of Combustor Parameters on the Combustion of Particle-Laden Fuels in Ducted Flows," AIAA Paper 73-177, Washington, D.C., 1973.

[3] Boussios, A., "Primärkammerprozesse für Kombinationsantriebe," Kursus der Carl-Cranz-Gesellschaft über "Flugkörperantriebe" in Braunschweig, March 19-23, 197?.

[4] McLain, W.H., "Identification of Exhaust Species from the combustion of LM and LMH Fuels," AFRPL TR-68-105, April 1968, Air Force Rocket Propulsion Lab., Edwards Air Force Base, Calif.

[5] Markowskii, L.Ya. and Kondrashev, Yu.D., "The composition and Properties of Borides of the Elements of the first and second Groups of the periodic Systems," *Zhurnal Neoranicheskoi Khimii*, Vol. 11, No. 1, 1957, pp. 34-41.

[6] Secrist, Childs, US Atomic Energy Rept. TID-17149, 1962.

[7] Hsia, H., "Air-Augmented Combustion of Boron and Boron-Metal Alloys," Final Rept. AFR DL-TR-71-80, June 1971, Air Force Research Lab., Wright-Patterson Air Force Base, Ohio.

Detection of Boundary-Layer Transition with a Laser Beam

A. J. Laderman* and A. Demetriades†
Aeronutronic Ford Corporation, Newport Beach, Calif.

Introduction

SEVERAL techniques, including surface sensors,[1] external probes[2,3] and optical methods[3,4] have been used for detection of transition in high speed, compressible boundary layers. While the various techniques yield useful information, each is deficient in some respect. Surface sensors, for example, respond only to phenomena adjacent to the wall, while probes (e.g. hot-wires) must be considerably smaller than the boundary-layer thickness δ in order not to disturb the local flow. Optical methods (schlieren, shadowgraph) are generally only qualitative in nature.

This Note describes an alternative scheme which overcomes these limitations. It involves the use of a laser beam in place of conventional optics, whose distortion by turbulence can be quantitatively linked to transition. Since the beam does not disturb the flow and can be focused to a region much smaller than δ it has potential for probing the entire transition region with high resolution. The feasibility of the method has been demonstrated using a helium-neon laser, with a beam approximately 1 mm diam, directed through a Mach 3 boundary layer. The beam axis is aligned parallel to the floor of the wind tunnel over which the boundary layer is growing and normal to the direction of mean flow, and is imaged on the plane of an apertured detector. In the direction of light propagation, therefore, the mean flow is uniform while both the mean flow and optical gradients are large in the direction normal to the wall and to the light beam.

Analysis

To assess the effects of turbulence on the optical quality of the beam, it can be assumed that the beam has a Gaussian

Received March 13, 1975; revision received July 14, 1975.

Index categories: Boundary Layers and Convective Heat Transfer—Turbulent; Boundary Layer Stability and Transition; Supersonic and Hypersonic Flow.

*Principal Scientist, Experimental Fluid Mechanics Section. Member AIAA.

†Supervisor, Experimental Fluid Mechanics Section. Associate Fellow AIAA.

distribution of intensity $I(x)$ which can be expressed as

$$I(x) = I_0 e^{-x^2/k^2} \tag{1}$$

where x is the distance normal to the beam axis, and k is a characteristic beam width. Upon emerging from the scattering region, each beam element oscillates due to the turbulent density fluctuations. The instantaneous position of such an element on the receiving detector is given by $x = \bar{x} + \Delta x(t)$ where $\bar{x}$ is the mean distance between the element and the beam axis, $\Delta x(t)$ is the instantaneous fluctuation, $\Delta x \ll \bar{x}$, and $\overline{\Delta x} \equiv 0$. Substituting into Eq. (1), expanding the exponential, and neglecting higher order terms, the time *average* intensity is given by

$$\overline{I(x)} = I(\bar{x}) \left[1 + \left(\overline{(\Delta x)^2}/k^2 \right) \left((2\bar{x}^2/k^2) - 1 \right) \right] \tag{2}$$

The instantaneous fluctuation intensity is defined as $\Delta I \equiv I(x) - \overline{I(x)}$ Squaring ΔI, taking the mean, and retaining only the lowest-order terms, we obtain the mean-square *intensity fluctuation* $\overline{(\Delta I)^2}$ and thus its rms value

$$\Delta I_{\text{rms}} \equiv \left(\overline{(\Delta I)^2} \right)^{1/2} = 2I(\bar{x}) \left(\overline{(\Delta x)^2}/k^2 \right)^{1/2} |\bar{x}/k| \tag{3}$$

Note that since, from Eq. (1), $\partial I/\partial x = -2\bar{x} I(\bar{x})/k^2$, we can also express Eq. (3) as

$$\Delta I_{\text{rms}} = \left(\overline{(\Delta x)^2} \right)^{1/2} |\partial I(\bar{x})/\partial x| \tag{4}$$

where in Eqs. (3) and (4) the absolute value of $\bar{x}$ and $\partial I(\bar{x})/\partial x$ must be used in order that ΔI_{rms} remain positive.

It is clear from the foregoing that the magnitude of the effects of turbulence on the mean intensity and the mean square intensity fluctuation are controlled by the ratio $\overline{(\Delta x)^2}/k^2$ and that for the geometry under consideration fluctuations will be detectable only where there are gradients in the undisturbed (incident) beam profile. Equations (2) and (3) reveal, in fact, all major effects of turbulence such as beam attenuation [put $\bar{x} = 0$ in (2)], spreading [put $\bar{x} > k/\sqrt{2}$ in (2)], defocusing (see Eq. (4)), loss of contrast and so on.

Experimental Apparatus

The experimental set-up is shown in Fig. 1. A 5 mw helium-neon laser was located within a few inches of the wind tunnel side window and the beam propagated through the floor boundary layer. The beam passed over a total path length ℓ of 24 meters to a 0.3 mm diam pinhole, located on the vertical beam centerline, and a 6328°A filter positioned immediately in front of a photomultipler tube. The aperture was attached to a motorized traversing mechanism which had a 2.5 cm total travel in the vertical direction. Due to the inherent beam divergence of the laser, the total beam size expanded to approximately 2.5 cm at the plane of the receiving aperture. The signal from the PM tube was fed simultaneously to: a) an rms meter, whose output in turn was fed to the Y input of an X-Y plotter to provide a record of ΔI_{rms}; b) the Y input of a second X-Y plotter to provide a record of the average intensity $\overline{I(x)}$; and c) to an oscilloscope to permit continuous monitoring of the signal. A voltage signal proportional to aperture position was fed to the X input of the recorders to provide directly the spatial distribution of ΔI_{rms} and $\overline{I(x)}$.

Results and Discussion

Measurements were made at several stations downstream of the nozzle throat. At each station, a tare or "noise" measurement of ΔI_{rms} and $\overline{I(x)}$ was made by installing in the test section a hollow cylinder coaxial with the beam centerline in order to shield the beam from the air flow. The tube was then removed and tests performed at various tunnel stagnation pressures, P_0. At the highest pressure the boundary layer throughout most of the tunnel was turbulent. As the pressure was reduced it became transitional and eventually laminar, with the maximum pressure able to sustain laminar flow decreasing with increasing distance from the throat. Typical curves of $\overline{I(x)}$ vs $\bar{x}$ are shown in Fig. 2 and the corresponding distributions of ΔI_{rms} are presented in Fig. 3. The experimental results show clearly the features predicted by Eqs. (2) and (3) and, in particular, that ΔI_{rms} has the double-peaked characteristic indicated by Eq. (3). It is also seen from Fig. 2 that $\overline{I(x)}$ is independent of operating conditions, and therefore that attenuation of the beam due to turbulent scattering is negligible in this case. That is, for the particular test conditions chosen, the values of $\overline{(\Delta x)^2}$, k, etc., are suitable for detecting the effects of Eq. (3) rather than those of Eq. (2).

A plot of the peak value of ΔI_{rms} vs P_0 obtained from measurements made at stations 16 and 28 cm downstream of the throat, is shown in Fig. 4. These stations are located within the acceleration section of the nozzle where the freestream Mach numbers are respectively 2.6 and 2.95, still lower than the test section value of 3. For these cases Fig. 4 indicates that: a) for laminar flow (low P_0), ΔI_{rms} is essentially zero (i.e., equal to the noise signal) implying vanishingly small fluctuations; and b) ΔI_{rms} reaches a maximum when the boundary-layer flow is transitional then diminishes for fully turbulent flow. It should be recalled that the overshoot in

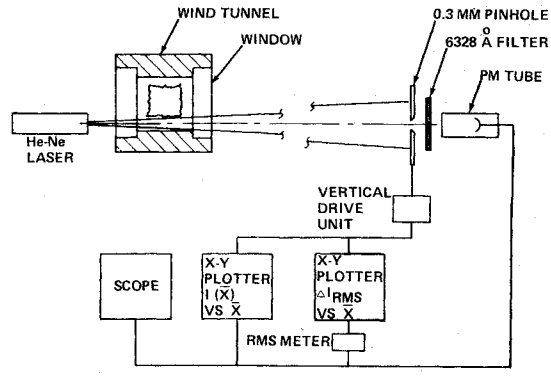

Fig. 1 Experimental set-up for laser detection of boundary-layer transition.

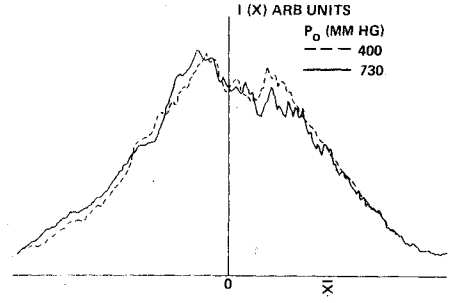

Fig. 2 Typical profiles of mean beam intensity.

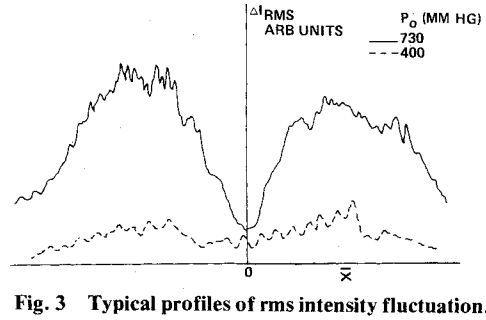

Fig. 3 Typical profiles of rms intensity fluctuation.

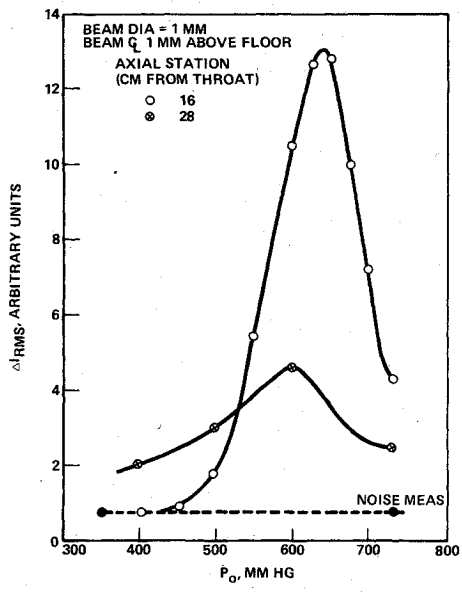

Fig. 4 Variation of peak rms intensity fluctuation with tunnel pressure.

fluctuation intensity, and therefore in ΔI_{rms}, is characteristic of transitional boundary-layer flow. In fact, the present results are remarkably similar to those obtained by Owen,[1] who used surface mounted hot film sensors to detect transition in supersonic boundary layers.

A comparison of the effect predicted by Eq. (3) and the experimental measurements is made using data obtained in the test section for fully-developed turbulence at a tunnel pressure $P_0 = 730$ mm Hg. For air, the variation in index of refraction Δn can be related to changes in density $\Delta\rho$ as follows

$$\Delta n = 0.000294\ \Delta\rho/\rho_0 = 0.00294\ (\Delta\rho/\rho)\ (\rho/\rho_0)$$

For $M_\infty = 3$ the freestream density, expressed in terms of the stagnation density (which in this case is nearly equal to the density at NTP), is $\rho_\infty = 0.076\ \rho_0$ while for the adiabatic case the density at the wall, as assuming constant static pressure across the boundary layer and a recovery factor near unity, is $\rho_w = \rho_0 p_w/p_0 = 0.027\ \rho_0$. Since the beam was located at about 0.3δ from the tunnel floor, we will use $\bar{\rho} \approx 0.05\rho_0$ and assume from Kistler's measurements[5] that the rms density fluctuation, normalized by the local mean, is 5%, yielding $\overline{(\Delta n)^2} \approx 5.5 \times 10^{-13}$. From Sutton's simplified scattering model,[6] the mean square angular fluctuation of a light ray traversing the turbulent boundary layer can be expressed as:

$$\overline{(\Delta\theta)^2} = \pi\overline{(\Delta n)^2}\ L/\Lambda$$

so that for out experiment

$$\overline{(\Delta x)^2} = \overline{(\Delta\theta)^2}\ \ell^2 = \pi\overline{(\Delta n)^2}\ L\ell^2/\Lambda$$

where L, the boundary-layer width = 7.5 cm, ℓ the optical path length = 24 m, and Λ, the turbulent scale length $= \delta/5 \simeq 0.1$ cm.[7] Substituting the appropriate values into the previous expression, we obtain

$$\left(\overline{(\Delta x)^2}\right)^{1/2} = \Delta x_{rms} \simeq 0.028 \text{ cm}$$

The parameter k is found by differentiating Eq. (3) with respect to $\bar{x}$ and setting $d(\Delta I_{rms}) = 0$. Thus $k = \sqrt{2}\bar{x}$, where $\bar{x}$ is the position for which ΔI_{rms} is a maximum. From the present tests this occurs at $\bar{x} = 0.6$ cm, so that $k = 0.84$ cm and from Eqs. (3) $I'\ (\equiv \Delta I_{rms}/I(\bar{x}))$ is 0.047 while from the experimental measurements $I' = 0.01$. The observed effect, therefore, is no more than a factor of 5 away from the prediction of Eq. (3). Of course, this discrepancy is symptomatic of the approximations in the analysis forced by incomplete knowledge of optical scattering[6] and of the details of supersonic turbulence. The important point is that the quantity I', whether equal to 0.01 or 0.05, is actually large enough to be measured simply even by unsophisticated laboratory set-ups. Another important point is that the actual magnitude of the sudden increase in I' (as shown on Fig. 4, for instance) at transition is not important to the detection of the transition point or region, an advantage common to other transition-detection methods as well.

Conclusions

We conclude from these results that a rather simple method of transition detection with a laser beam is available. The remote-sensing nature of the technique makes it attractive for use in ground tests, expecially if the beam can be made to pass through a width of the layer several times its thickness. The results are sufficiently encouraging to warrant an extension of the tests just described into the lower Mach number regime.

References

[1] Owen, F. K., "Transition Experiments on a Flat Plate at Subsonic and Supersonic Speeds," *AIAA Journal*, Vol. 8, March 1970, pp. 518-523.

[2] Potter, J. L. and Whitfield, J. D., "Effects on Slight Nose Bluntness and Roughness on Boundary Layer Transition in Supersonic Flows," *Journal of Fluid Mechanics*, Vol. 12, Pt. 4, April 1962, pp. 501-535.

[3] Demetriades, A., "Hypersonic Viscous Flow Over a Slender Cone, Part III: Laminar Instability and Transition," AIAA Paper 74-535, Palo Alto, Calif., 1974.

[4] Fischer, M. C. and Weinstein, L. M., "Cone Transitional Boundary Layer Structure at $M_e = 14$," *AIAA Journal*, Vol. 10, May 1972, pp. 699-701.

[5] Kistler, A. L., "Fluctuation Measurements in a Supersonic Trubulent Boundary Layer," *Physics of Fluids*, Vol. 2, No. 3, May-June 1959, pp. 290-296.

[6] Sutton, G. W., "Effect of Turbulent Fluctuations in an Optically Active Fluid Medium," *AIAA Journal*, Vol 7, Sept. 1969, pp. 1737-1743.

[7] Laderman, A. J. and Demetriades, A., "Mean and Fluctuating Flow Measurements in the Hypersonic Boundary Layer Over a Cooled Wall," *Journal of Fluid Mechanics*, Vol. 63, Pt. 1, March 1974, pp. 121-144.

Convergence of an Iterative Procedure for Large-Scale Static Analysis of Structural Components

F. Austin* and I. U. Ojalvo†
Grumman Aerospace Corporation, Bethpage, N. Y.

Introduction

CONDITIONS for convergence have been derived for an iterative procedure, proposed by Newman and Goldberg,[1] which is currently being employed to efficiently determine static stresses in the space-shuttle thermal protection system.[2] This procedure can also be used effectively for the analysis of other built-up component structures in which one of the substructures possesses a dominant stiffness which largely influences the deformations of the entire system. The general idealization being considered is represented in Fig. 1.

Received April 7, 1975; revision received July 23, 1975. This work was performed for the NASA Langley Research Center under contract NAS 1-10635.

Index categories: Structural Static Analysis; Thermal Stresses.

*Engineering Group Specialist, Structural Mechanics Section.

†Structural Mechanics Engineer